A Micellar Sphere-to-Cylinder Transition of Poly(ferrocenyldimethylsilane-*b*-2-vinylpyridine) in a Selective Solvent Driven by Crystallization

Lei Shen,[†,‡] Hai Wang,[‡] Gerald Guerin,[‡] Chi Wu,[§] Ian Manners,*[,‡,||] and Mitchell A. Winnik*[,‡]

Department of Chemistry, University of Toronto, 80 St. George Street, Toronto, Ontario, Canada M5S 3H6, The Hefei National Laboratory for Physical Sciences at Microscale, Department of Chemical Physics, University of Science and Technology of China, Hefei 230026, Anhui, China, Department of Chemistry, The Chinese University of Hong Kong, Shatin, N. T., Hong Kong, and School of Chemistry, University of Bristol, Bristol BS8 1TS, U.K.

ABSTRACT: A sample of poly(ferrocenyldimethylsilane)-*b*-poly(2-vinylpyridine) (PFS$_{23}$-*b*-P2VP$_{230}$), with a short PFS block and a P2VP block 10-fold higher in degree of polymerization, forms spherical micelles when dissolved in ethanol. Over time (hours, days, and weeks), these solutions undergo a micelle sphere-to-cylinder transition eventually forming rather stiff, uniform fiber-like micelles with a core width of 10 nm, lengths between 20 and 50 μm, and approximately four polymer molecules per nm length. Here, we report the results of a combination of transmission electron microscopy, wide-angle X-ray scattering (WAXS), as well as static and dynamic laser light scattering measurements to follow the structural evolution. One key observation is the onset of partial aggregation of spherical micelles after an initial induction period (hours), so that the system as it ages consists of mixtures of free spherical micelles, micelle aggregates, and elongated structures with a high aspect ratio. Another important observation is the growth in intensity and sharpness of the WAXS peak characteristic of crystalline PFS domains as the number and uniformity of the cylindrical micelles increases. This formation of crystalline domains is the likely driving force for the structural transformation.

Introduction

Amphiphilic block copolymers self-assemble in selective solvents to yield a range of supramolecular morphologies, such as spherical micelles, cylinders, lamellae and vesicles.[1–7] The size and shape of aggregates obtained depend upon a number of factors, such as the relative block lengths of the polymers, the chemical nature of the blocks, the presence of additives (salts, homopolymers, etc.), solvent composition, and temperature. These structures, with nanometer dimensions, have a variety of applications such as supports for catalytic devices, drug delivery carriers, and lithographic templates.[8–16] As a consequence, the study of block copolymer self-assembly has attracted intense scientific and technological attention.

We are interested in organic−organometallic block copolymers in which the organometallic block contains a ferrocene in the backbone of the repeat unit.[17] One such set of polymers has poly(ferrocenyldimethylsilane) (PFS) as the insoluble block. These block copolymers are interesting in part because of the unique features of PFS homopolymer. This polymer can be oxidized to a semiconductor. Its thin films act as charge dissipative coatings, and its derivatives can be shaped and pyrolyzed to yield magnetic ceramics.[18–20] These polymers are also interesting because many compositions yield rod-like cylindrical micelles in solution. Examples include PFS-*b*-polydimethylsiloxane (PFS-*b*-PDMS),[21] PFS-*b*-polymethylvinylsiloxane (PFS-*b*-PMVS),[22] PFS-*b*-polyisoprene (PFS-*b*-PI),[23] and PFS-*b*-poly(methyl methacrylate) (PFS-*b*-PMMA).[24] We have provided evidence that the crystallization of the PFS core

polymer is the main driving force for the formation of the cylindrical morphologies in most of these polymers.[21–23]

There are other examples in which different morphologies are obtained. For example, one sample of PFS-*b*-polystyrene (PFS-*b*-PS) with a relatively short PS block was reported to form spherical micelles in acetone, a solvent selective for the short PS block.[25] PFS-*b*- poly(dimethylaminoethyl methacrylate) (PFS-*b*-PDMAEMA)[26] gave rod-like micelles in ethanol but more complicated morphologies in other solvents. Even more interesting is the case of PFS-*b*-poly(2-vinylpyridine) (PFS-*b*-P2VP).[27] We found that it formed spherical micelles in methanol and cylindrical structures in 2-propanol. We also mentioned on an observation that, when dissolved in ethanol, this polymer initially formed spherical micelles, but these micelles appeared to evolve into more elongated structures on standing. This paper reports the results of a more detailed examination of this morphology rearrangement for the specific case of PFS$_{23}$-*b*-P2VP$_{230}$, where the subscripts refer to the number average degree of polymerization.

There are many examples in the literature of sphere-to-cylinder transformations of self-assembled structures. The earliest reference, for traditional small molecule surfactants, is the work of Luzzati et al.[28] Since then, this topic has been thoroughly investigated.[29] For most traditional surfactants, an increase in concentration or temperature results in the formation of elongated micelles.

This type of transition has also been observed in polymer systems, which show more complex behavior than the conventional surfactants. For instance, both Chu's group[30] and Brown's group[31] used laser light scattering (LLS) to investigate the sphere-to-cylinder transition of poly(ethylene oxide)−poly-(propylene oxide)−poly(ethylene oxide) (PEO−PPO−PEO) triblock copolymers induced by an increase in temperature in dilute aqueous solution. Mortensen et al.[32] also studied this

* To whom correspondence should be addressed. Email: mwinnik@chem.utoronto.ca. (M.W.); ian.manners@bristol.ac.uk. (I.M.).
† University of Science and Technology of China.
‡ University of Toronto.
§ The Chinese University of Hong Kong.
|| University of Bristol.

system using small-angle neutron scattering (SANS). Eisenberg and co-workers[33] examined the sphere-to-cylinder transition for poly(styrene)-*b*-poly(acrylic acid) (PS-*b*-PAA) block copolymers by varying the composition of a dioxane/water mixed solvent.

In addition, Möller's group[34] investigated micelle formation by poly(styrene)-*b*-poly(2-vinylpyridine) (PS-*b*-P2VP) in toluene for samples in which the insoluble P2VP block was significantly longer than the PS block. When the P2VP block was partially protonated by HAuCl$_4$, they observed a mixture of spheres and cylinders by transmission electron microscopy (TEM) and scanning force microscopy (SFM), and the spheres appeared to condense into cylinders. They suggested that the cylinders grew by deposition of spherical micelles onto their ends. Iyama et al.[35] reported that dilute solutions of certain poly(styrene)-*b*-poly(dimethyl siloxane) (PS-*b*-PDMS) samples underwent a structural rearrangement from spherical to cylindrical micelles upon heating. Lodge et al.[36] reported transitions between spheres, cylinders, and vesicles by varying the solvent composition for poly(styrene)-*b*-poly(isoprene) (PS-*b*-PI), and LaRue et al.[37] investigated the sphere-to-cylinder transition of PS-*b*-PI induced solely by temperature in heptane. Recently, Savin and co-workers[38] studied the cylinder-to-sphere transition of a poly(butadiene)−poly(L-lysine) amphiphilic block copolymer in water solution by changing the pH. A theoretical analysis by Linse et al.,[39] based on a mean-field lattice model, provided phase diagrams and a prediction for the locus of the sphere-to-cylinder transition in heterogeneous systems. Zhulina et al.[40] investigated dilute solutions of neutral diblock copolymer micelles from both experimental and theoretical points of view and demonstrated that transitions between spherical and cylindrical micelle morphologies occur in or near the crew-cut regime of block copolymer composition.

In the experiments cited in the previous paragraph, all of the cylindrical micelles reported were formed from block copolymers, in which the core-forming block was comparable in length or longer than the corona-forming soluble block. Here, we report a study by TEM, wide-angle X-ray scattering (WAXS), as well as static (SLS) and dynamic (DLS) light scattering of a sphere-to-cylinder transition for micelles formed by PFS$_{23}$-*b*-P2VP$_{230}$, in ethanol, for which the degree of polymerization of the soluble block is a factor of 10 longer than that of the PFS block. This transition, which occurs on a timescale of weeks, is likely driven by the crystallization of the PFS component in solution.

Experimental Section

Materials. *n*-Decane (99+%), toluene (99.8%), and ethanol (100%) were purchased from Aldrich and used without further purification. The synthesis and characterization of block copolymer PFS$_{23}$-*b*-P2VP$_{230}$ was described in ref 27. It was synthesized by multiple-stage anionic polymerization, beginning with dimethylsilaferrocenophane initiated by *n*-butyllithium and subsequent addition of 1,1-dimethylsilacyclobutane, 1,1-diphenylethylene, and 2-vinylpyridine. The reaction was terminated with degassed methanol. The copolymer was purified by repeated size exclusion column chromatography using tetrahydrofuran as the eluent. In that publication, the molar mass of the PFS block was determined by size exclusion chromatography (SEC) with reference to polystyrene (PS) standards and the composition (i.e., the block ratio) was determined by ^{1}H NMR. Massey et al.[41] have shown that SEC based upon PS standards underestimates the molar mass of PFS polymers, but their work did not extend to samples as small as that employed here for the PFS block. Additional ^{1}H NMR experiments (see Figure S1 in Supporting Information) reported here show that values of M_n can be determined by end group analysis (the CH$_3$ group of the butyllithium initiator). In this way, we determined M_n(PFS) = 5600, M_n(copolymer) = 30 000, and M_w/M_n = 1.07.

The polydispersity of the block copolymer was determined by triple detection (TD-SEC). In ref 27, this polymer was described as PFS$_{17}$-*b*-P2VP$_{170}$.

Sample Preparation. Polymer solutions for LLS experiment were prepared by mixing PFS$_{23}$-*b*-P2VP$_{230}$ with ethanol followed by filtration through 0.20 μm PTFE membranes. Samples were aged in the dark at 20 °C. Aliquots for TEM analysis were taken at various time intervals. One sample carefully sealed in a stoppered flask was aged for more than one year in the dark at ambient temperature (ca. 23 °C).

Laser Light Scattering. A modified commercial light scattering spectrometer (ALV/SP-125) equipped with an ALV-5000 multitau digital time correlator and a He−Ne laser (output power = 35 mW at λ_0 = 632.8 nm) was used. In static light scattering (SLS), we obtained both the weight-average molar mass (M_w) and the *z*-average root-mean-square radius of gyration ($\langle R_g^2 \rangle^{1/2}$) of scattering objects in a dilute solution from the scattering vector (*q*) dependence of the excess absolute scattering intensity, known as the Rayleigh ratio $R(q)$

$$KC/R(q) = (1 + \langle R_g^2 \rangle q^2/3)/M_w + 2A_2C \qquad (1)$$

where $K = 4\pi^2 n^2 (dn/dC)^2/(N_A\lambda_0^4)$, $q = (4\pi n/\lambda_0)\sin(\theta/2)$, and N_A, n, λ_0, and θ are the Avogadro number, the solvent refractive index, the wavelength of the light in vacuum, and the scattering angle, respectively. The extrapolation to $C \rightarrow 0$ and $q \rightarrow 0$ leads to M_w. Plots of $[KC/R(q)]_{C\rightarrow 0}$ versus q^2 and $[KC/R(q)]_{C\rightarrow 0}$ vs C lead to $\langle R_g^2 \rangle$ and A_2, respectively. For block copolymers, the specific refractive index increment $(dn/dC)_{polymer}$ is related to the dn/dC values of the components via the weight fractions w_j of monomer type *j* in the polymer (with $\Sigma_{j=1} w_j = 1$):

$$(dn/dC)_{polymer} = \sum_{j=1} w_j (dn/dC)_j \qquad (2)$$

provided that the dn/dC contributions of the multicomponent polymer in a single solvent are additive. Using values of $(dn/dC)_{PFS}$ = 0.253 mL/g and $(dn/dC)_{P2VP}$ = 0.245 mL/g in ethanol, we calculated $(dn/dC)_{polymer}$ = 0.2464 mL/g.

For small scattering objects, the Zimm plot on the basis of eq 1 is usually used, which incorporates the extrapolations of $C \rightarrow 0$ and $q \rightarrow 0$ in a single grid. For elongated structures, as cylindrical micelles, the particle scattering form factor $P(q) = (R(q)/KCM_w)_{C\rightarrow 0}$ can be plotted as $qP(q)/\pi$ versus $\langle R_g \rangle q$ according to the Casassa−Holtzer analysis.[42] The simplest approach for $P(q)$ analysis of stiff thin rods with monodisperse length *L* is given by

$$P(q) = (2/qL)\int_0^{qL} [\sin(qL)/qL]\, d(qL) - [(2/qL)\sin(qL/2)]^2 \qquad (3)$$

To accommodate polydispersity in this presentation for a system of cylinders, polydisperse in length, a weight average Zimm−Schulz distribution[43]

$$w(L) = b^{z+1} L^z e^{-bL}/z! \qquad (4)$$

was used together with $b = (z + 1)/L_w$. *z* and L_w are the polydispersity index ($z = 1/[(L_w/L_n) - 1]$) and weight averaged contour length of the cylinders, respectively.

In dynamic light scattering (DLS), the Laplace inversion of each measured intensity−intensity time correlation function $[(G^{(2)}(q,\tau) - B)/B]$ of scattering objects in a dilute solution can lead to a line-width distribution ($G<\Gamma>$), where *B* is the measured baseline. The CONTIN Laplace inversion program in the correlator software was used. For a pure diffusive relaxation, Γ is related to the translational diffusive coefficient (*D*) by $D = (\Gamma/q^2)_{q\rightarrow 0, C\rightarrow 0}$ and further to the hydrodynamic radius (R_h) by $R_h = k_B T/(6\pi\eta D)$, where k_B, η, and *T* are the

Boltzmann constant, the solvent viscosity, and the absolute temperature, respectively. Therefore, $G(\Gamma)$ can be converted to a distribution of translational diffusion coefficients ($G(D)$) or a hydrodynamic radius distribution ($f(R_h)$). For large particles, Γ/q^2 shows a q-dependence in the low q range limit given by the equation:

$$\langle\Gamma\rangle/q^2 = D_t(1 + C_\Gamma\langle R_g^2\rangle q^2 - ...) \qquad (5)$$

where D_t is the translational diffusion coefficient and C_Γ is a parameter that depends upon the molecular architecture and polydispersity of the particles.

In the current study, all measurements were carried out at 20.00 ± 0.05 °C. Two angular ranges were investigated. The first range consisted of scattering angles between 20° and 30° (at 2° intervals), while the other range consisted of angles between 30° and 150° (at 5° intervals). Some experiments were carried out at a fixed scattering angle of 17.0°. SLS and DLS measurements were carried out simultaneously. Filtered toluene was used as the standard solvent in the SLS experiments.

Transmission Electron Microscopy. Dark field transmission electron microscopy (TEM) images were taken using a Hitachi HD-2000 STEM instrument operating at 200 kV and 13 μA current. For TEM samples, a polymer solution was dropped onto a carbon-coated copper grid, and then transferred to the TEM after the liquid dried completely.

Wide-Angle X-ray Scattering. Samples for wide-angle X-ray scattering (WAXS) measurements were prepared by casting a film from a micelle solution (1.0×10^{-3} g/mL) in ethanol at 20 °C onto a silicon substrate followed by spontaneous evaporation of the solvent. WAXS diffraction data were obtained with a Siemens D500 $\theta/2\theta$ diffractometer with a Cu Kα source operating at 50 kV and 35 mA in the step scan mode.

Results and Discussion

In a previous publication,[27] we reported that the PFS-P2VP polymer examined here (PFS$_{23}$-b-P2VP$_{230}$, PFS:P2VP block ratio 1:10, $M_n = 30\,000$, $M_w/M_n = 1.07$) formed spherical micelles in methanol and cylindrical structures in 2-propanol. Both types of structures are characterized by a dense PFS core and a corona of P2VP chains. Films formed from the cylindrical micelles exhibited a prominent WAXS peak at 6.4 Å, characteristic of (semi)crystalline PFS, whereas the WAXS spectrum of a film formed from the spherical micelles in methanol showed no features. We suggested that the spherical micelles were formed under kinetic control and that the enhanced solubility of the block copolymer in 2-propanol facilitated nucleation and growth of the cylindrical structures. The idea of enhanced solubility was based on solubility parameter (δ) arguments. The value of the solubility parameter of PFS ($\delta_{PFS} = 18.7$ MPa$^{1/2}$)[44] is closer to that of 2-propanol ($\delta_{2\text{-PrOH}} = 23.5$ MPa$^{1/2}$) than to that of methanol ($\delta_{MeOH} = 29.7$ MPa$^{1/2}$). As a less poor solvent for PFS than methanol, 2-propanol improves its solubility and allows the PFS to rearrange into crystallized structures. The solubility parameter of P2VP is 21.7 MPa$^{1/2}$, which suggests that 2-propanol is also a better solvent for the corona chains than methanol.

Ethanol has a solubility parameter ($\delta_{EtOH} = 26.0$ MPa$^{1/2}$) intermediate in magnitude between those of 2-propanol and methanol for both PFS and for P2VP. Upon dissolution in this solvent, PFS$_{23}$-b-P2VP$_{230}$ forms spherical micelles that over time evolve to cylindrical structures. We begin our description of this morphology evolution by examining TEM images and laser light scattering data for samples at the two extremes of the morphology evolution: spherical micelles examined shortly after sample preparation and cylindrical micelles in a sample carefully aged for one year.
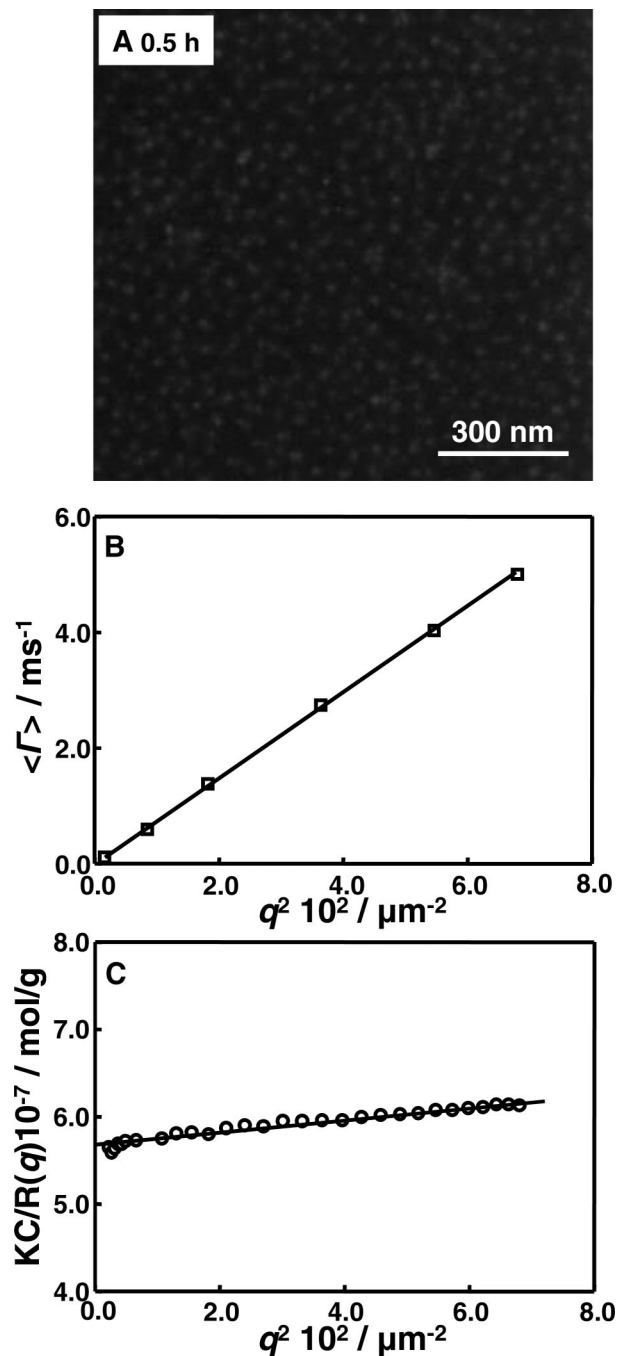
Figure 1. (A) Dark-field TEM micrographs depicting structure evolution for a sample of PFS$_{23}$-b-P2VP$_{230}$ diblock copolymer in ethanol (1.0×10^{-4} g/mL) 0.5 h after sample preparation. (B) Scattering vector (q^2) dependence of the average characteristic line-width ($<\Gamma>$) of the same polymer solution at the same time after sample preparation. (C) A typical Zimm plot for this solution.

Spherical Micelles in Freshly Prepared Solutions. When samples of PFS$_{23}$-b-P2VP$_{230}$ were added to dry ethanol, transparent solutions formed upon swirling the mixture at 20 °C. TEM images of films formed from these solution shortly after sample preparation reveal the presence of only spherical micelles, quite uniform in size with an average core diameter of ca. 25 nm. An example from a droplet of solution (1.0×10^{-4} g/mL) placed on the TEM grid 0.5 h after sample preparation is shown in Figure 1A. Because of the low contrast between the supporting carbon film and the P2VP corona, the spheres on the TEM images are expected to represent only the PFS iron-rich core region of the micelles.
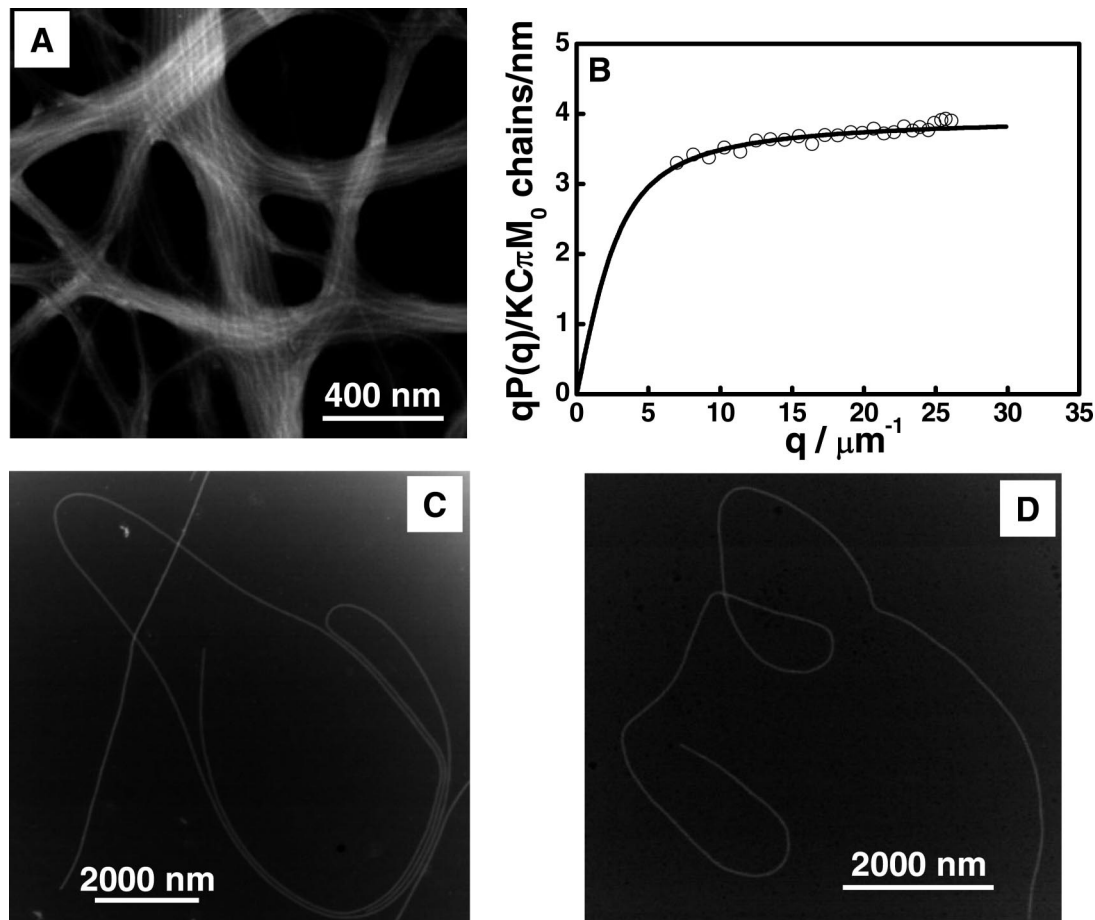
Figure 2. (A) Dark-field TEM micrographs depicting structure evolution for a sample of PFS$_{23}$-*b*-P2VP$_{230}$ diblock copolymer in ethanol (1.0 × 10^{-4} g/mL) 1 year after sample preparation. (B) Plot of qR(q)/KCπM$_0$ as a function of q for a diluted solution of these micelles diluted 20-fold and then sonicated for 3 min. The fitted line yields L_w = 800 nm, M_w = 1.02 × 10^8 g/mol, L_w/L_n = 1.5. (C) and (D) Dark-field TEM micrographs of the same solution examined in (B) prior to sonication.

Dynamic (DLS) and static (SLS) light scattering measurements were carried out on the same solution of PFS$_{23}$-*b*-P2VP$_{230}$ block copolymer in ethanol at 20 °C. These experiments give information about shape, size, and molar mass of the scattering objects present in solution.[45–47] The polymer solution was filtered through a 0.20 μm PTFE membrane to remove the dust, and the first data points were collected at the same time (after 0.5 h) that the sample for TEM was prepared. DLS and SLS data were collected simultaneously. A plot of the DLS line-width $<\Gamma>$ vs q^2 is presented in Figure 1B. A straight line passing through the origin reveals that the relaxation measured for the small micelles is purely diffusive, and a spherical shape can be inferred from the independence of $<\Gamma>/q^2$ on q^2. The calculated hydrodynamic radius ($\langle R_h \rangle$ = 25 nm) is larger than the core radius seen in the TEM image (Figure 1A), because the P2VP corona contributes to R_h in the DLS measurement but offers little contrast in the TEM experiment. At this low concentration, there is no concentration dependence detected on the apparent R_h value.

In the SLS experiment carried out at the same time, a typical Zimm plot was obtained (Figure 1C). The extrapolated value of $[R(q)/KC]_{q\to0}$ leads to an apparent $M_{w,app}$, which, because of the small concentration effect in the dilute regime, is likely close to the absolute M_w of the micelle. Using a value of (dn/dC)$_{polymer}$ = 0.2464 mL/g in ethanol, we calculate M_w of 1 760 000 g/mol for these spherical micelles. By comparison with the PFS$_{23}$-*b*-P2VP$_{230}$ molar mass, we deduce that the micelles have a mean apparent aggregation number N_{app} (= $M_{w,app}/M_{w,chain}$) of ca. 55. From the slope of the plot, we obtained the z-average root-

mean-square radius of gyration ($\langle R_g \rangle \approx$ 20 nm). It is known that for a flexible random coil chain in an athermal solvent $\langle R_g \rangle /\langle R_h \rangle \approx$ 1.5 and for a uniform hard sphere $\langle R_g \rangle /\langle R_h \rangle$ = 0.774.[46] The value $\langle R_g \rangle /\langle R_h \rangle \approx$ 0.8 obtained here is consistent with the idea that PFS$_{23}$-*b*-P2VP$_{230}$ chains form relatively uniform spherical micelles upon dissolution in ethanol.

Cylindrical Micelles after a Year. A solution of PFS$_{23}$-*b*-P2VP$_{230}$ at the same concentration (1.0 × 10^{-4} g/mL) was carefully stored for one year at room temperature (ca. 23 °C) in the dark, with no significant loss of solvent. The dark-field TEM image in Figure 2A shows that only long fiber-like structures were present. Here one sees bright filaments with a uniform diameter of 10 nm, which we ascribe to the PFS cores of these micelles, flanked by lighter gray regions, which are likely due to the P2VP coronae. Not only are the PFS cores of uniform width but also they appear as evenly spaced parallel lines within these fiber bundles. The equal distance between adjacent fibers that is probably determined by the space occupied by P2VP chains. We estimate the edge-to-edge distance between adjacent fibers as ca. 20 nm. This compares with an estimated end-to-end distance for the P2VP segments of about 10 nm.[48] There was no indication of residual spherical micelles. In order to observe individual fibers more clearly, we diluted the solution 20 times and examined them at lower magnification. Although all of the images showed elongated fibers, most of the fibers extended outside the image area, and it was not possible to measure their length with any confidence. In Figure 2C,D, we present images of two individual fiber-like micelles, which are
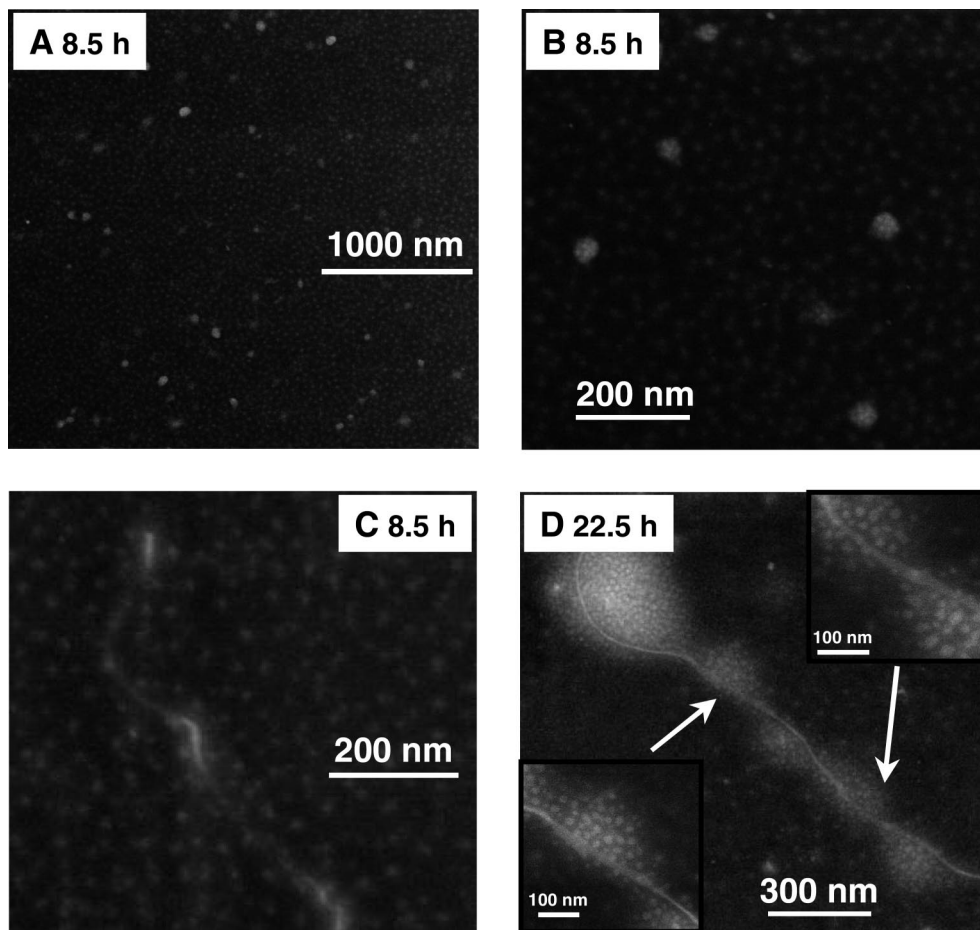
Figure 3. Dark-field TEM micrographs depicting structure evolution for a sample of PFS$_{23}$-*b*-P2VP$_{230}$ diblock copolymer in ethanol (1.0 × 10^{-4} g/mL). A-C) 8.5 h later. (B) and (C) refer to two different locations on the same TEM grid. (D) The same solution after 22.5 h.

sufficiently coiled that the entire length lies in the image frame. We estimate that for all of these micelles the length ranged from about 20 to 50 μm, much longer than the "giant fiber-like" block copolymer micelles reported by other groups.

SLS measurements on these diluted solutions (5.0 × 10^{-6} g/mL) were problematic. Scattering data from long thin objects are normally plotted as a Casassa–Holtzer representation ($qR(q)/KC$ vs q) and exhibit a plateau at high q.[49–51] Some experiments gave reasonable plots in which values of $qR(q)/KC$ were independent of q over the entire range of accessible angles, as might be expected for such long fibers. Other measurements gave scattered data and, upon visual inspection, one could see that the laser beam did not pass uniformly through the solution. To overcome problems associated with the very long lengths of the fibers, the diluted solution was subjected to 3 min exposure to a 90 W ultrasonic bath, the conditions which we in the past have shown to lead to fragmentation (shortening) of PFS cylindrical micelles without affecting their width. These solutions well behaved in the light scattering experiments. Data obtained in this way are plotted in Figure 2B, and in terms of the units employed for the y-axis of these plots, ($qR(q)/KC\pi M_0$), the magnitude of the plateau is given in polymer molecules per nm of rod length. The solid line corresponds to the best fit of the data to the form factor for thin rigid rods as per eq 3. The value of the plateau does not depend on chain length (L_w) or the polydispersity (L_w/L_n) of the cylinders.[52] In order to test the robustness of the fit for the plateau, we fixed L_w to various values in the range of 800–1000 nm and fitted the data to obtain corresponding L_w/L_n and plateau values. While the values of L_w/L_n changed, we obtained the same value of the plateau as shown in Figure S2 in Supporting

Information. Thus we deduce that there are approximately 4 polymer chains per nm.

The Morphology Transition Observed by TEM. Our focus here is on the nature of the structural evolution, which from a TEM perspective, we examine through the images presented in Figures 3 and 4. In Figure 3, we show the objects present in a sample taken after 8.5 and 22.5 h at 20 °C. In the low magnification dark-field TEM image presented in Figure 3A, one can see well-spaced bright spots with diameters on the order of 50–60 nm. When seen at higher magnification (Figure 3B,C), three types of structures can be discerned. First, there is a background of spherical micelles, too small to be noted in Figure 3A, which resemble the micelles seen in Figure 1A.

In Figure 3B, these are accompanied by circular objects that are light gray in color, with diameters of about 60 nm. Each of these contains a countable number (on the order of 10) of bright spots comparable in size to individual spherical micelles outside these larger objects. While we cannot say for certain whether these are spheres or disks, they appear to be aggregates of micelles. This is the most common feature of the TEM images at this resolution. Nevertheless, other features can be discerned. As shown in Figure 3C, there are regions of the grid that contain a small number of short elongated micelles of relatively uniform width (10 nm), with lengths that range from 30 to 90 nm.

There is also an indication of much thinner connecting fibers between the ends of the elongated structures. The number of these objects is very small, and the predominant structures present in the solution, as discerned from the TEM images, are the spherical micelles with diameters of ca. 25 nm.
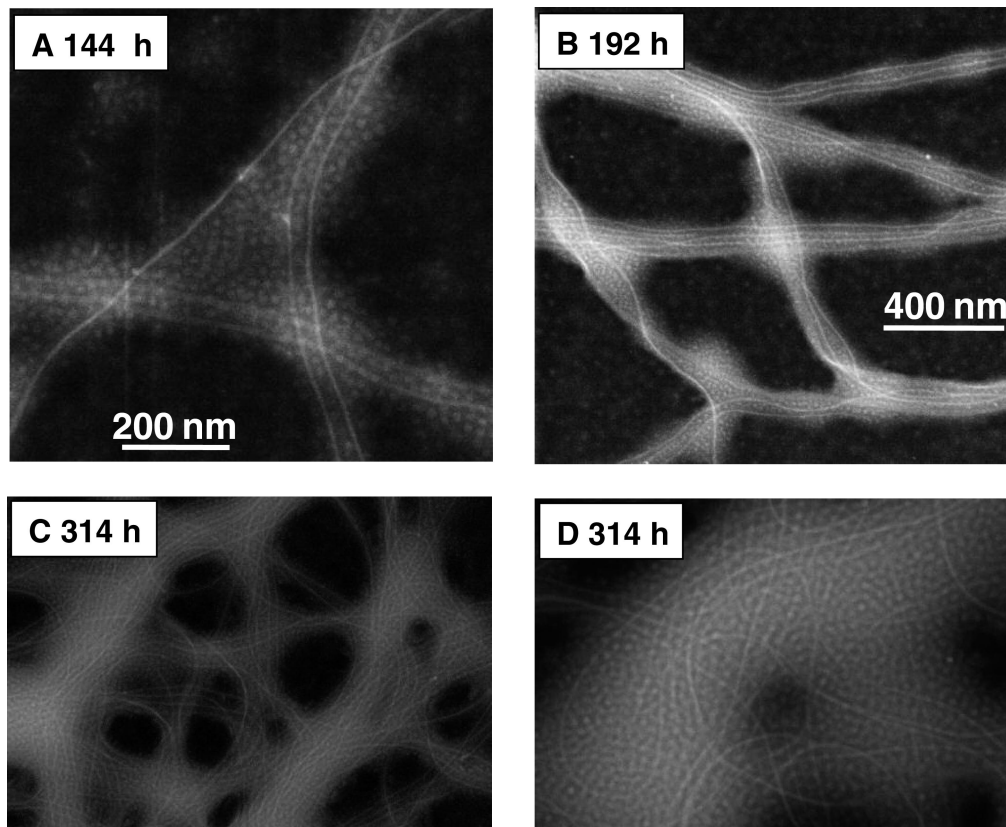
Figure 4. Dark-field TEM micrographs depicting structure evolution for a sample of PFS_{23}-b-$P2VP_{230}$ diblock copolymer in ethanol (1.0×10^{-4} g/mL) aged for different times at 20 °C: (A) 144 h; (B) 192 h; (C, D) 314 h at two different levels of magnification.

In Figure 3D, we show a TEM image taken 22.5 h after sample preparation. One sees the presence of elongated structures, coexisting with spherical micelles. A qualitative examination of a series of micrographs obtained from this solution shows that the length of the fibers is on the order of $1-2$ μm, 50 times larger than the diameter of spherical micelles. As indicated in the two insets of higher magnification, many small bright objects, presumably spherical micelles or their aggregates, tend to cluster alongside the fibers. These clusters may be a consequence of sample drying on the TEM grid, but they may also reflect an intermediate stage of the morphology transformation in solution. Interestingly, a variation in width can be observed along the fibers. While much of the fiber length appears relatively uniform in width (10 nm), there are regions in the insets to Figure 3D where widths up to 20 nm can be seen. It is interesting to note that the width of these fibers is smaller than the 25 nm diameter of the spherical micelles. Since there is much less contrast for P2VP than PFS with the carbon-coated TEM grid, we infer that the bright domains seen in these dark-field TEM images are PFS domains of the micelles. Dense P2VP domains are probably the source of the faint gray background separating the brighter small PFS spheres and PFS fibers seen in these images.

For the samples aged 144 and 192 h, there are an increasing number of rather stiff fiber-like structures as shown in panels A and B of Figure 4, respectively. Many of the cylinders are $5-10$ μm long. Close inspection shows a large number of seemingly unchanged spherical micelles in the background. The images in Figure 4C,D (314 h) are interesting in this respect. At low magnification, the spherical micelles cannot be seen,

but at higher magnification (Figure 4D), one can see that a large number of these micelles accompany the fiber-like structures that dominate the lower resolution image. Only after a year do we obtain a sample that is free of any indication of these spherical micelles. Even after 18 months, these solutions remained colloidally stable; no precipitates were ever observed.

Wide-Angle X-ray Scattering (WAXS) Measurements. We have argued in the past[21–23] that the defining characteristic of PFS block copolymers that form cylindrical micelles is the crystallinity of the PFS in the core of the cylinders. PFS itself is a (semi)crystalline polymer,[53,54] and its films exhibit a characteristic peak in the WAXS spectrum corresponding to a spacing of 6.36 Å. In the single-crystal study of the PFS pentamer, this peak corresponds to a 6.287 Å spacing between adjacent planes of the fully extended molecules.[55] We have also noted that films formed from cylindrical micelles of PFS_{23}-b-$P2VP_{230}$ in 2-propanol gave a single strong reflection corresponding to a spacing of 6.4 Å,[27] whereas films formed from the spherical micelles that formed in methanol gave no discernible WAXS peak.

In order to examine whether crystallization of the PFS played a role in the sphere-to-cylinder transition of PFS_{23}-b-$P2VP_{230}$ in ethanol, we carried out WAXS measurements on films formed from solutions aged for 0.5, 24, 192 h, and 1 year. As shown in Figure 5, no peak can be detected in the sample aged 30 min, indicating that the initially formed spherical micelles contain amorphous PFS chains. In contrast, a weak peak having a d spacing of 6.4 Å appeared in the WAXS spectrum of films formed by PFS_{23}-b-$P2VP_{230}$ micelles aged in ethanol for 24 h.
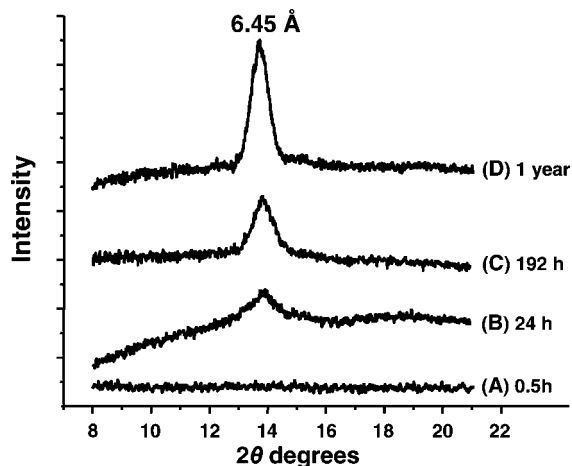
Figure 5. WAXS pattern for films of PFS$_{23}$-b-P2VP$_{230}$ micelles prepared from an ethanol solution (1.0×10^{-3} g/mL) aged for different times at 20 °C: (A) 30 min after sample preparation; (B) after 24 h; (C) after 192 h; (D) after 1 year.
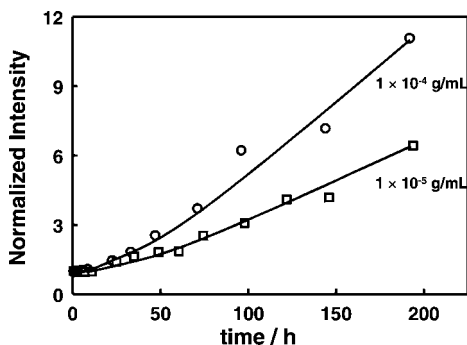
Figure 6. Evolution of the normalized light scattering intensity of ethanol solutions of PFS$_{23}$-b-P2VP$_{230}$ at two different concentrations (1.0×10^{-4} and 1.0×10^{-5} g/mL) at 20.00 °C. The scattering angle is 17.00°.

In a sample from a solution aged just over a week (192 h), this peak became stronger. For the solution that was aged for 1 year, this peak sharpened considerably, with a maximum at 6.45 Å. This information is consistent with the idea that crystallization of the PFS chains accompanies the formation of cylindrical micelles and is likely the driving force for the sphere-to-cylinder transition of PFS$_{23}$-b-P2VP$_{230}$ block copolymers in ethanol. Nevertheless, the width of the WAXS peak and the lack of higher order peaks suggest that the degree of crystallinity in these samples is small.

Laser Light Scattering Measurements. With increasing time, these spherical micelles transform into cylindrical structures. The larger structures are much more visible in light scattering, because the scattering intensity (I) is proportional to the square of the mass of (M) of scattering objects, i.e., $I \sim M^2$. Figure 6 shows the growth in normalized scattering intensity of the PFS$_{23}$-b-P2VP$_{230}$ solution at two different polymer concentrations. The scattered intensity at a 17.0° scattering angle was obtained as the number counts obtained in a fixed time window. These data were normalized by dividing them by the intensity of the incoming laser beam. Over the first 5 h, little increase of I was observed. After about 10 h, one can see the onset of an increase in scattering intensity, corresponding to a growth in the overall weight-averaged micelle mass (M). The increase at 10 h is relatively small and corresponds to the time for which we see a small number of circular clusters and short elongated structures in the TEM (Figure 3A−C).
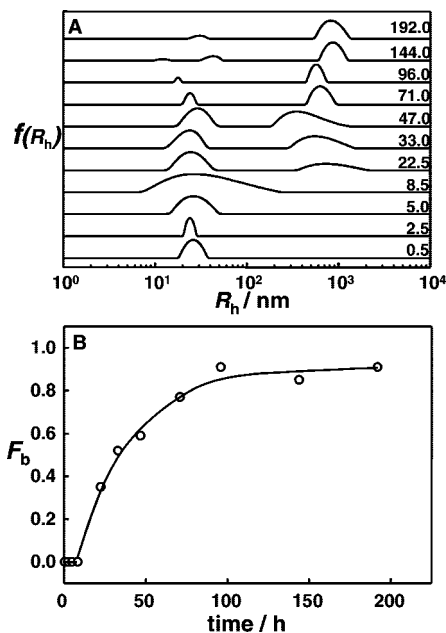
Figure 7. A) Hydrodynamic radius distributions ($f(R_h)$) of a PFS$_{23}$-b-P2VP$_{230}$ solution in ethanol (1.0×10^{-4} g/mL) with increasing aging time. The scattering angle is 17.0°. (B) The area fraction (F_b) corresponding to the slow mode in (A) plotted as a function of aging time.

Dynamic Light Scattering (DLS). DLS measurements carried out on solutions undergoing structural evolution exhibit two relaxation modes in $G(\Gamma)$. These indicate the coexistence of self-assembled structures of two distinct sizes. CONTIN plots of the hydrodynamic radius distribution ($f(R_h)$), obtained from DLS measurements on the PFS$_{23}$-b-P2VP$_{230}$ ethanol solution at 1.0×10^{-4} g/mL are presented in Figure 7A. Over the first 8.5 h, $f(R_h)$ is unimodal. Nevertheless, $f(R_h)$ broadens significantly, indicating the presence of both spherical micelles and aggregates of micelles. The solution at 8.5 h described here is the same solution used to obtain the TEM images seen in Figure 3A−C. Thus, we can identify the source of broadening in $f(R_h)$ as due to the presence of the spherical aggregates seen in Figure 3B as well as the short elongated aggregates seen in Figure 3C. At 22.5 h, $f(R_h)$ changes from unimodal to bimodal, as expected for a mixture of spherical and rod-like micelles. With further aging, the mode corresponding to the longer relaxation time grows bigger, indicating that more and more spherical micelles have been transformed into cylindrical structures. We also carried out similar experiments for a lower concentration (1.0×10^{-5} g/mL) sample of PFS$_{23}$-b-P2VP$_{230}$ in ethanol (not shown) and obtained qualitatively similar results.

In a DLS experiment, the integrated area under a $G(\Gamma)$ distribution is proportional to the excess scattered intensity $R(q)$ over solvent. For a mixture of two different objects in the same solution, if there exist two distinct peaks in $G(D)$, denoted as $G_a(D)$ and $G_b(D)$, the area ratio (A_r) of these two peaks can be written as

$$A_r = A_b/A_a = F_b/(1 - F_b) = \left[\int_0^\gamma G_b(D)\, dD\right]/\left[\int_\gamma^\infty G_a(D)\, dD\right]$$

$$= (M_{w,b}x_b)/(M_{w,a}x_a) \qquad (6)$$

where the subscripts "a" and "b" denote the two different objects and γ is the cutoff translational diffusion coefficient between $G_a(D)$ and $G_b(D)$. X_a and X_b are weight fractions of the objects (a and b). The term $F_b = A_b/(A_a + A_b)$ plotted in Figure 7B describes the fraction of scattering intensity due to the large slow moving species seen as the slow mode in Figure 7A. After
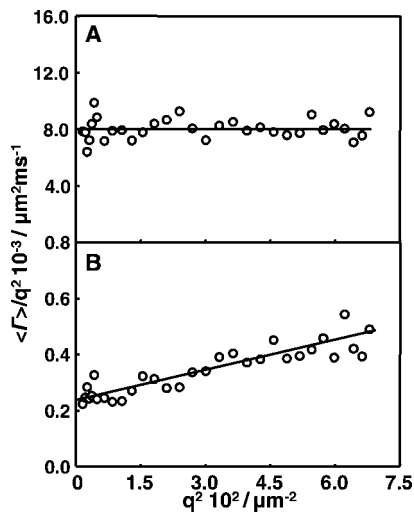
Figure 8. Dependence of $<\Gamma>/q^2$ on q^2 for a solution of PFS$_{23}$-b-P2VP$_{230}$ (1.0×10^{-4} g/mL) in ethanol aged 192 h at 20.00 °C: (A) the fast relaxation mode in $G(\Gamma)$; (B) the slow relaxation mode.

100 h aging, the larger objects in the solution contribute more than 80% of the scattering intensity. Unfortunately, these data do not allow us to calculate the mass fraction of the two components, because we do not know $M_{w,b}$ of the species corresponding to the slow relaxation time peak in Figure 7A.

Taking the 192 h solution as an example, plots of $<\Gamma>/q^2$ vs q^2 for each mode are shown in Figure 8. The intensity–intensity time correlation functions at two q values (17° and 150°) for this solution are shown in Figure S3 in Supporting Information. For the fast relaxation mode, $<\Gamma>/q^2$ is independent of q^2 (Figure 8A), consistent with the contribution of spherical and optically isotropic particles. In contrast, the positive slope for the slow mode in the $<\Gamma>/q^2$ on q^2 plot (Figure 8B) indicates a polydisperse system or a system exhibiting a rotational contribution to diffusion. We attribute this relaxation to the presence of elongated micelles in our system because, at large scattering angles for dilute solutions of long cylinders, an additional exponential decay appears in the correlation function representing local motions, especially rotation.

Static Light Scattering (SLS). In Figure 9A, we present Zimm plots ($KC/R(q)$ vs q^2) for polymer solutions at different aging times of the SLS data obtained simultaneously with the DLS measurements. The upper line (0.5 h) corresponds to the Zimm plot presented in Figure 1B. Only spherical micelles are present. With increasing aging time, the data exhibit a steep initial part at low scattering angles and a flatter curvature at large scattering angles. The downward type of curvature is often indicative of the presence of elongated objects in the solution,[56] which we attribute to the rod-like micelles in our system. The flatter portion of these curves at large scattering angles, on the other hand, arises from the presence of the smaller spherical micelles. This superposition of scattering from elongated objects and much smaller species has analogies to the work of Herzog et al.,[57] who used light scattering to examine the growth of semiflexible rod-like aggregates in aqueous NaCl solutions from monomeric dye molecules. In our experiments, no further insights are available into the nature of the larger, elongated species, if we attempt to correct the data in Figure 9A to remove the contribution of scattering by the spherical micelles. When the data in Figure 9A are replotted as a Casassa–Holtzer representation ($qR(q)/KC$ vs q), we obtain the results shown in Figure 9B. From the positive slopes, we learn that the form factor has a stronger q dependence than predicted for rigid thin cylinders, as shown in Figure 2B. While a unique interpretation of these plots is not possible, we suggest that aggregates, perhaps
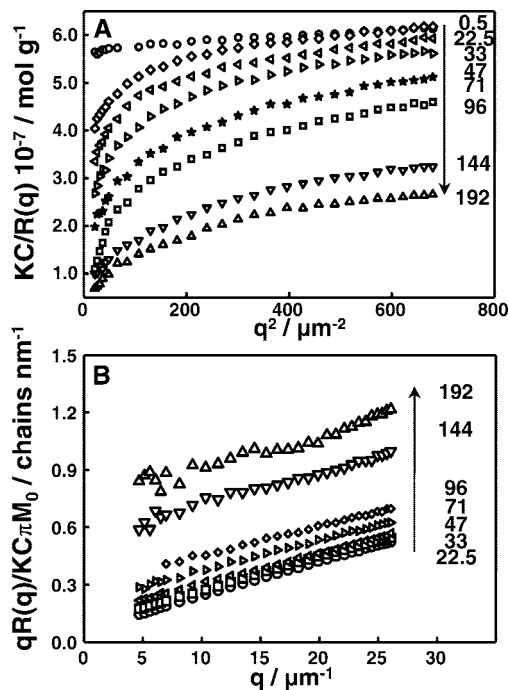
Figure 9. (A) Plots of $KC/R(q)$ as a function of q^2 for a solution of PFS$_{23}$-b-P2VP$_{230}$ in ethanol (1.0×10^{-4} g/mL) at 20.00 °C for different aging times. (B) Replotting of the data in (A) as a Casassa–Holtzer representation $qR(q)/KC$ vs q.

similar to those observed in the TEM images in Figure 4B,C, are present in solution and contribute to the scattering signal.

Mechanism of the Sphere-to-Cylinder Transformation. One of the important characteristics of the morphology transformation described above is the onset of partial aggregation of spherical micelles after an initial induction period (hours). Aggregated structures coexist with small spherical micelles throughout the structure transformation process until, after a year, all low-aspect-ratio species have disappeared from the solution. Another important characteristic is the increase in the extent of crystallinity of the PFS as the transformation proceeds. The WAXS peaks seen in Figure 5 increase in intensity and sharpen as the solution ages. The challenge for us is to connect these observations into a mechanism for the sphere-to-cylinder transformation in this system.

We begin by recalling that PFS$_{23}$-b-P2VP$_{230}$ forms small spherical micelles in methanol similar in size to those formed initially in ethanol. In methanol, no aggregation is seen by DLS and no structural evolution is seen by TEM over a period of a week. This result implies that the spherical micelles themselves are colloidally stable as long as the spherical PFS domain remains amorphous. From this perspective, the crystallization of the PFS core in the core of a spherical micelle can be seen as a rare event that occurs more rapidly in ethanol than in methanol. We hypothesize that once this crystallization occurs, the micelle becomes colloidally unstable. When these structures encounter one another in solution, they form aggregates. The circular objects seen in Figure 3A,B would then be aggregates of spherical micelles with a semicrystalline core.

It is interesting for us to note that the diameter of the core (ca. 25 nm) for the small spherical micelles is similar in size to the spherical polyethylene domains in the polyethylene-b-poly(styrene-r-ethylene-r-butene) (E/SEB) melts studied by Loo et al.[58] For sufficiently strong segregation, these domains crystallized under the confinement of the amorphous rubbery block, preserving the bcc lattice structure of the material. These domains underwent homogeneous nucleation, and exhibited first-order kinetics in the

crystal growth. For polymers with a higher volume fraction of the ethylene block, the extent of confinement imposed by the matrix was less. Crystalline material from individual domains was able to "break out" to encounter neighboring domains and nucleate crystallization. These authors studied crystallization kinetics at a variety of temperatures. We note that, in their systems, the crystallization processes they deemed to be slow (over 3–4 h) are still much faster than that reported here.

We like this concept of breakout and use this idea to suggest that occasionally the PFS cores of the spherical aggregates seen in Figure 3B break out to form a single localized PFS domain, which then becomes elongated as seen in Figure 3C. Thin protrusions of PFS appear to connect these domains. We imagine from the image seen in Figure 3D for the sample aged 22.5 h that spherical micelles begin to aggregate along these protrusions to give the fiber–cluster aggregates seen in the insets to this figure. Transfer of material within the aggregates leads to local regions of the fibers that are wider than the equilibrium structure. Upon ripening, the PFS cores of the cylindrical micelles reach their ultimate width of 10 nm. Eventually, the system evolves to a mixture of cylindrical micelles, spherical micelles, and their aggregates. The CONTIN plots in Figure 7A indicate that even after 192 h there are still free spherical micelles in the system.

At some point there has to be a crossover in growth mechanism. We know that the cylindrical micelles formed by this PFS$_{23}$-*b*-P2VP$_{230}$ polymer in 2-propanol can be "chain extended" by introducing to the micelle solution additional polymer dissolved in a common good solvent like tetrahydrofuran. Addition of this polymer does not lead to the formation of new cylindrical micelles but rather leads to an increase in length of the micelles already present in solution.[59] We have referred to this process as "living self-assembly", in analogy with living polymerization reactions, and have explored its properties in a more detailed study of other PFS block copolymer in selective solvents.[60] To maintain consistency with this well-documented behavior, we have to assume that at some point in sample aging, the growth of the cylindrical micelles occurs only at the ends. We see no indication that this occurs by collision of small spherical micelles with the ends of the cylindrical structures. We previously showed that solutions of short cylindrical micelles of PFS–polyisoprene in decane kept their length and relatively narrow length distribution when aged 5 months at room temperature.[60] End-to-end aggregation in this system did not occur. This result argues against growth involving interaction of the cylindrical micelle ends with preexisting micelles. It is more likely that growth occurs via the slow dissociation of individual molecules from the spherical micelles or their aggregates into the solution and incorporation onto the cylinder ends by epitaxial crystallization onto the exposed ends of the PFS core. From this perspective, the presence of aggregates as seen in the TEM images at 144, 192, and 314 h play no role in the micelle growth process.

Our model for the sphere-to-cylinder transformation presumes that nucleation occurs over a period of tens of hours in ethanol and involves rare events such as that seen in Figure 3D. This is followed by an extended growth period lasting up to one year. Solvent must play an important role in both the nucleation step and the subsequent growth process. Methanol, the poorest solvent for PFS, shows no evidence of nucleation over a period of 1 week. This effect may be related to the fact that the experimental temperature (20 °C) is close to the glass transition temperature (T_g = 33 °C) for PFS homopolymer.[17–23] The short chain length of the PFS block likely leads to a core-polymer T_g below room temperature; nevertheless, the mobility of PFS chains in the core may be restricted by the proximity to T_g. In 2-propanol, a less poor solvent for PFS, nucleation and growth are rapid. After a day, the solution consists entirely of cylindrical micelles with lengths on the order of a few μm. From this result, we infer that many nuclei form over a relatively short time scale.

While we have not yet examined the growth kinetics in 2-propanol, we suggest that the micelles grow in length over a period of hours.

Ethanol is an intermediate quality solvent for PFS. Here, we know that spherical micelles are formed initially and presume that solvent penetration into the PFS core assists the onset of crystallization. It must also promote dissolution of free chains in the continuous medium to permit the growth of the cylindrical micelles. From the extraordinary length of the fiber-like micelles seen after one year (ca. 20 to 50 μm), we infer that nucleation events are rare and the nuclei formed grow into very long micelles.

Summary

Using a combination of TEM, WAXS and laser light scattering, we have examined the sphere-to-cylinder transition for micelle solutions of PFS$_{23}$-*b*-P2VP$_{230}$ block copolymer in ethanol. The small spherical micelles formed initially ($\langle R_h \rangle$ = 25 nm, $\langle R_g \rangle \approx$ 20 nm, aggregation number 55 molecules per micelle) resemble the stable micelles formed by this polymer in methanol. Over time, the solution becomes enriched in cylindrical micelles and aggregates of spherical structures with these elongated objects. After one year, the solution contains only long thin micelles with a uniform core width of 10 nm, lengths ranging from 20 to 50 μm, and approximately 4 polymer molecules per nm length. These resemble the somewhat shorter cylindrical micelles formed by this polymer in 2-propanol. Normally, block copolymers with long corona chains and short insoluble blocks prefer to form spherical star-like micelles to take advantage of the sharp curvature of small spheres that minimizes corona chain repulsion in a good solvent. For PFS$_{23}$-*b*-P2VP$_{230}$ with a much long corona-forming chain, some other factor such as the crystallization of the core polymer must drive the transformation to a cylindrical structure with a smaller core diameter than that of the precursor spherical micelles and larger repulsion between corona chains.

Although the TEM images provide a rich view of changes in the system over time, the detailed mechanism of the sphere-to-cylinder transition remains obscure. In refs 59 and 60, we showed that once seed micelles are present, they grow by deposition of polymer molecules onto the ends of these structures. Thus, we imagine from the 20 to 50 μm length of the cylindrical micelles present in our solutions after one year that nucleation is a rare event and micelle growth is slow. This means that the various aggregates detected by light scattering and seen in by TEM at intermediate times are not important intermediates in cylinder growth. These aggregates serve as a reservoir for block copolymer molecules, which have rather poor solubility in the medium. As individual polymer molecules slowly dissociate from the spherical micelles or aggregates, they become incorporated into the cylinder micelles by epitaxial crystallization onto the ends of the PFS block. More experiments are needed to understand the details of the cylinder nucleation process.

References and Notes

(1) Hamley, I. W. *The Physics of Block Copolymers*; Oxford University Press: Oxford, London, 1998.

(2) Hadjichristidis, N.; Pispas, S.; Floudas, G. A. *Block Copolymers*; Wiley: New York, 2003.

(3) Discher, D. E.; Eisenberg, A. *Science* **2002**, *297*, 967.

(4) Riess, G. *Prog. Polym. Sci.* **2003**, *28*, 1107.

(5) Forster, S.; Abetz, V.; Müller, H. E. *Adv. Polym. Sci.* **2004**, *166*, 173.

(6) Gohy, J. F. *Adv. Polym. Sci.* **2005**, *190*, 65.

(7) Rodriguez-Hernandez, J.; Checot, F.; Gnanou, Y.; Lecommandoux, S. *Prog. Polym. Sci.* **2005**, *30*, 691.

(8) Aleshin, A. N. *Adv. Mater.* **2006**, *18*, 17.

(9) Chan, V. Z.-H.; Hoffman, J.; Thomas, E. L. *Science* **1999**, *286*, 1716.

(10) Forster, S.; Antonietti, M. *Adv. Mater.* **1998**, *10*, 195.

(11) Hamley, I. W. *Angew. Chem., Int. Ed.* **2003**, *42*, 1692.

(12) Stupp, S. I.; LeBonheur, V.; Walker, K.; Li, L. S.; Huggins, K. E.; Keser, M.; Amstutz, A. *Science* **1997**, *276*, 384.

(13) Gref, R.; Minamitake, Y.; Peracchia, M. T.; Trubetskoy, V.; Torchilin, V.; Langer, R. *Science* **1994**, *263*, 1600.

(14) Schnerder, A.; Zanna, J.-J.; Yamada, M.; Finkelmann, H.; Thomann, R. *Macromolecules* **2000**, *33*, 649.

(15) Dalhaimer, P.; Bates, F. S.; Discher, D. E. *Macromolecules* **2003**, *36*, 953.

(16) Savic, R.; Luo, L. B.; Eisenberg, A.; Maysinger, D. *Science* **2004**, *300*, 615.

(17) Kulbaba, K.; Manners, I. *Macromol. Rapid Commun.* **2001**, *22*, 711.

(18) Peterson, R.; Foucher, D. A.; Tang, B. Z.; Lough, A.; Nandyala, R. P.; Greedan, J. E.; Manners, I *Chem. Mater.* **1995**, *7*, 2045.

(19) Rulkens, R.; Resendes, R.; Verma, A.; Manners, I.; Murti, K.; Fossum, E.; Miler, P.; Matyjaszewski, K. *Macromolecules* **1997**, *30*, 8165.

(20) Kulbaba, K.; Cheng, A.; Bartole, A.; Greenberg, S.; Resendes, R.; Coombs, N.; Safa-Sefat, A.; Greedan, J. E.; Stover, H. D. H.; Ozin, G. A.; Manners, I. *J. Am. Chem. Soc.* **2002**, *124*, 12522.

(21) (a) Massey, J.; Power, K. N.; Manners, I.; Winnik, M. A. *J. Am. Chem. Soc.* **1998**, *120*, 9533. (b) Massey, J.; Temple, K.; Cao, L.; Rharbi, Y.; Raez, J.; Winnik, M. A.; Manners, I. *J. Am. Chem. Soc.* **2000**, *122*, 11577. (c) Raez, J.; Manners, I.; Winnik, M. A. *J. Am. Chem. Soc.* **2002**, *124*, 10381. (d) Raez, J.; Zhang, Y.; Cao, L.; Petrov, S.; Erlacher, K.; Wiesner, U.; Manners, I.; Winnik, M. A. *J. Am. Chem. Soc.* **2003**, *125*, 6010.

(22) Wang, X.; Wang, H.; Frankowski, D. J.; Lam, P. G.; Welch, P. M.; Winnik, M. A.; Hartmann, J.; Manners, I.; Spontak, R. J. *Adv. Mater.* **2007**, *19*, 2279.

(23) (a) Cao, L.; Manners, I.; Winnik, M. A. *Macromolecules* **2001**, *34*, 3353. (b) Cao, L.; Massey, J. A.; Winnik, M. A.; Manners, I.; Riethmuller, S.; Banhart, F.; Spatz, J. P.; Möller, M. *Adv. Funct. Mater.* **2003**, *13*, 271.

(24) Korczagin, I.; Hempenius, M. A.; Fokkink, R. G.; Cohen Stuart, M. A.; Al-Hussein, M.; Bomans, P. H. H.; Frederik, P. M.; Vancso, G. J. *Macromolecules* **2006**, *39*, 2306.

(25) Massey, J.; Power, K. N.; Manners, I.; Winnik, M. A. *Adv. Mater.* **1998**, *10*, 1559.

(26) Wang, X.; Winnik, M. A.; Manners, I. *Macromolecules* **2005**, *38*, 1928.

(27) Wang, H.; Winnik, M. A.; Manners, I. *Macromolecules* **2007**, *40*, 3784.

(28) Reiss-Husson, F.; Luzzati, V. *J. Phys. Chem.* **1964**, *68*, 3504.

(29) (a) Hoffmann, H.; Ebert, G. *Angew. Chem., Int. Ed.* **1988**, *27*, 902. (b) Imae, T.; Skeda, S. *J. Phys. Chem.* **1986**, *90*, 5216. (c) Gamboa, C.; Rois, H.; Sepulveda, L. *J. Phys. Chem.* **1989**, *93*, 5540. (d) Christov, N. C.; Denkov, N. D.; Kralchevsky, P. A.; Ananthapad-manabhan, K. P.; Lips, A. *Langmuir* **2004**, *20*, 565. (e) Bernheim-Groswasser, A.; Zana, R.; Talmon, Y. *J. Phys. Chem. B* **2000**, *104*, 4005. (f) Alargova, R. G.; Danov, K. D.; Petkov, J. T.; Kralchevsky, P. A.; Broze, G.; Mehreteab, A. *Langmuir* **1997**, *13*, 5544. (g) Heerklotz, H.; Tsamaloukas, A.; Kita-Tokarczyk, K.; Strunz, P.; Gutberlet, T. *J. Am. Chem. Soc.* **2004**, *126*, 16544.

(30) Zhou, Z.; Chu, B. *Macromolecules* **1988**, *21*, 2548.

(31) (a) Schillen, K.; Brown, W.; Johnsen, R. M. *Macromolecules* **1994**, *27*, 4825. (b) Jorgensen, E. B.; Hvidt, S.; Brown, W.; Schillen, K. *Macromolecules* **1997**, *30*, 2355.

(32) Mortensen, K.; Pedersen, J. S. *Macromolecules* **1993**, *26*, 805.

(33) (a) Zhang, L.; Eisenberg, A. *Science* **1995**, *268*, 1728. (b) Burke, S. E.; Eisenberg, A. *Langmuir* **2001**, *17*, 6705.

(34) Spatz, J. P.; Möβmer, S.; Möller, M. *Angew. Chem., Int. Ed.* **1996**, *35*, 1510.

(35) Iyama, K.; Nose, T. *Polymer* **1998**, *39*, 651.

(36) Lodge, T. P.; Bang, J.; Li, Z.; Hillmyer, M. A.; Talmon, Y. *Faraday Discuss.* **2005**, *128*, 1.

(37) LaRue, I.; Adam, M.; Pitsikalis, M.; Hadjichristidis, N.; Rubinstein, M.; Sheiko, S. *Macromolecules* **2006**, *39*, 309.

(38) Gebhardt, K. E.; Ahn, S.; Venkatachalam, G.; Savin, D. A. *Langmuir* **2007**, *23*, 2851.

(39) Linse, P. *J. Phys. Chem.* **1993**, *97*, 13896.

(40) Zhulina, E. B.; LaRue, I.; Sheiko, S. S.; Rubinstein, M. *Macromolecules* **2005**, *38*, 5330.

(41) Massey, J.; Kulbaba, K.; Winnik, M. A.; Manners, I. *J. Polym. Sci., Part B: Polym. Phys.* **2000**, *38*, 3032.

(42) (a) Holtzer, A. *J. Polym. Sci.* **1955**, *17*, 432. (b) Casassa, E. F. *J. Am. Chem. Soc.* **1956**, *78*, 3980.

(43) Zimm, B. *J. Chem. Phys.* **1948**, *16*, 1099.

(44) Kulbaba, K.; MacLachlan, M. J.; Evans, C. E. B.; Manners, I. *Macromol. Chem. Phys.* **2001**, *202*, 1768.

(45) Chu, B. *Laser Light Scattering*, 2nd ed.; Academic Press: New York, 1991.

(46) Berne, B.; Pecora, R. *Dynamic Light Scattering*; Plenum Press: New York, 1976.

(47) Burchard, W. In *Light Scattering Principles and Development*; Clarendon Press; Brown, W.; Oxford 1996; p 439.

(48) Brandrup, J.; Immergut, E. H.; Grulke, E. A. *Polymer Handbook*, 4 th ed.;Wiley: New York, 1999; p VII-58.

(49) Schmidt, M.; Paradossi, G.; Burchard, W. *Makromol. Chem. Rapid Commun.* **1985**, *6*, 767.

(50) Denkinger, P.; Burchard, W.; Kunz, M. *J. Phys. Chem.* **1989**, *93*, 1428.

(51) Guerin, G.; Raez, J.; Manners, I.; Winnik, M. A. *Macromolecules* **2005**, *38*, 7819.

(52) Denkinger, P.; Burchard, W. *J. Polym. Sci., Part B: Polym. Phys.* **1991**, *29*, 589.

(53) Rasburn, J.; Petersen, R.; Jahr, T.; Rulkens, R.; Manners, I.; Vancso, G. J. *Chem. Mater.* **1995**, *7*, 871.

(54) (a) Chen, Z.; Foster, M. D.; Zhou, W.; Fong, H.; Reneker, D. H.; Resendes, R.; Manners, I. *Macromolecules* **2001**, *34*, 6156. (b) Papkov, V. S.; Gerasimov, M. V.; Dubovik, I. I.; Sharma, S.; Dementiev, V. V.; Pannell, K. H. *Macromolecules* **2000**, *33*, 7107.

(55) Rulkens, R.; Lough, A. J.; Manners, I.; Lovelace, S. R.; Grant, C.; Geiger, W. E. *J. Am. Chem. Soc.* **1996**, *118*, 12683.

(56) Savin, G.; Burchard, W. *Macromolecules* **2004**, *37*, 3005.

(57) Herzog, B.; Huber, K.; Stegemeyer, H. *Langmuir* **2003**, *19*, 5223.

(58) Lou, Y-L.; Register, R. A.; Ryan, A. J. *Macromolecules* **2002**, *35*, 2365.

(59) Wang, H.; Lin, W.; Fritz, K. P.; Scholes, G. D.; Winnik, M. A.; Manners, I. *J. Am. Chem. Soc.* **2007**, *129*, 12924.

(60) Wang, X.; Guerin, G.; Wang, H.; Wang, Y.; Manners, I.; Winnik, M. A. *Science* **2007**, *317*, 644.